Characterization of HCC mouse models: Towards an etiology-oriented subtyping approach

Running title: Subtyping HCC mouse models

Juliane Friemel[1]*, Lukas Frick[1,2]*, Kristian Unger[3], Michele Egger[1], Rossella Parrotta[1], Yannick T. Böge[1], Arlind Adili[1], Michael Karin[4], Tom Luedde[5], Mathias Heikenwalder[6*], Achim Weber[1*]

[1] Department of Pathology and Molecular Pathology, University and University Hospital Zurich, Zurich, Switzerland

[2] Swiss Hepato-Pancreato-Biliary Center, Department of Digestive and Transplant Surgery, University Hospital of Zurich, Zurich, Switzerland

[3] Helmholtz Zentrum München Research Center for Environmental Health (GmbH), Research Unit Radiation Cytogenetics

[4] Department of Pathology, University of California, San Diego, California, USA

[5] Department of Medicine III, University Hospital RWTH Aachen, Aachen, Germany.

[6] Division Chronic Inflammation and Cancer, German Cancer Research Center, Heidelberg, Germany

*JF and LF share first authorship, AW and MH share last authorship

Key words

Hepatocellular carcinoma, mouse models, liver carcinogenesis, intratumor heterogeneity, synteny analysis

Financial support

AW was supported by a grant from the Swiss Cancer League (Oncosuisse). MH was supported by an ERC Consolidator grant (HepatoMetaboPath); the DKFZ MOST program, the SFB 209 and the HepCAR 2020. TL was supported by Mildred-Scheel Endowed Professorship from the German Cancer Aid (Deutsche Krebshilfe) and the German Research Foundation (DFG) (LU 1360/3-1 and SFB-TRR57/P06).

Corresponding authors

Achim Weber, Department of Pathology and Molecular Pathology, University and University Hospital Zurich, Zurich, Switzerland

Achim.weber@usz.ch Tel: +41 442552781

Mathias Heikenwalder, Division Chronic Inflammation and Cancer, German Cancer Research Center, Heidelberg, Germany

m.heikenwaelder@dkfz.de Tel: +49 6221423891

Conflict of interest

The authors disclose no conflict of interest.

Acknowledgements

The results published here are in whole or part based upon data generated by the TCGA Research Network: http://cancergenome.nih.gov/."

Word counts

Abstract: 243

Main manuscript: 3275

Abstract

Murine liver tumors often fail to recapitulate the complexity of human hepatocellular carcinoma (HCC), which might explain the difficulty to translate preclinical mouse studies into clinical science. The aim of this study was to evaluate a subtyping approach for murine liver cancer models with regard to etiology-defined categories of human HCC; comparing genomic changes, histomorphology and immunohistochemistry profiles. Sequencing and analysis of gene copy number changes (by CGH) in comparison with etiology-dependent subsets of HCC patients of the TCGA database was conducted using specimens (75 tumors) of five different HCC mouse models: di-ethyl-nitrosamine [DEN]-induced wild type C57BL/6 mice, c-Myc and AlbLTαβ transgenic mice as well as TAK1^{LPC-KO} and Mcl-1$^{\Delta hep}$ mice. Digital microscopy was used for assessment of morphology and immunohistochemistry of liver cell markers (A6-CK7/19, glutamine synthetase) in mouse and n=61 human liver tumors. Tumor CGH-profiles of DEN-treated mice and c-Myc transgenic mice matched alcohol-induced HCC, including morphological findings (abundant inclusion bodies, fatty change) in the DEN model. Tumors from AlbLTαβ transgenic mice and TAK1^{LPC-KO} models revealed the highest overlap with NASH-HCC CGH-profiles. Concordant morphology (steatosis, lymphocyte infiltration, intratumor heterogeneity) was found in AlbLTαβ murine livers. CGH profiles from the Mcl-1$^{\Delta hep}$ model displayed similarities with hepatitis induced HCC and characteristic human-like phenotypes (fatty change, inter- and intratumor heterogeneity). Our findings demonstrate that stratifying preclinical mouse models along etiology-oriented genotypes and human-like phenotypes is feasible. This closer resemblance of preclinical models is expected to better recapitulate HCC subgroups, and thus increase their informative value.

Background

Human HCC is the most common primary liver cancer and has become the third leading cause of cancer related death worldwide (1, 2). The main risk factors for liver carcinogenesis are chronic liver diseases such as viral hepatitis, alcoholic or nonalcoholic steatohepatitis (ASH/NASH), exposure to aflatoxin or genetic disposition (e.g. α1-antitrypsin deficiency) (3). Dietary induced liver cancer is an emerging problem in developed as well as in developing countries (4, 5).

Strategies to improve the still poor survival of HCC patients rely on preclinical mouse models, such as cell-line derived models in immunocompromised mice (allo- and xenografts), genetically engineered mouse models (GEMM) and environmentally induced models. So far, the translational value of mouse models with respect to patient benefit has frequently fallen behind the expectations. Besides the need for discovering new anti-HCC targets and compounds and testing them *in vivo*, it is of utmost importance to improve analyses and subtyping for preclinical mouse model research. First, distinct models may recapitulate only individual features of human HCC. Second, reporting of morphology, immunohistochemistry profiles, genetic landscapes, sequencing of the key tumor suppressors/oncogenes and growth monitoring of murine tumors is poorly standardized in mouse research (6). An important challenge in the comprehensive characterization of murine models is already to identify truly malignant lesions. Different criteria are used such as atypia, increased proliferation, expansive growth, necrosis or extracapsular invasion (7-9). Markers like glutamine synthetase and collagen IV may serve as supplemental indicators for tumor diagnosis (10-12). Mutational profiles of murine liver tumors, with

frequent *CTNNB1* mutations and rare or absent *TP53* alterations were characterized in earlier studies (13-15).

Approaches to improve mouse model characterization and subtyping include i) systematic assessment of human-like phenotypes including morphology, immunohistochemistry profiles and intratumor heterogeneity, ii) evaluation of etiology-dependent models, and iii) if possible assignment to a clinically stratified patient subgroup. The murine models analyzed in this study comprise four GEMMs and one environmentally induced model, all with spontaneous, orthotopic tumor growth. Different genetic backgrounds were included, covering essential cancerogenesis pathways (8, 10, 11, 16-18): oncogene overexpression (c-Myc), chronic inflammation (TAK1$^{LPC\text{-}KO}$ and AlbLTαβ) and liver cell loss with compensatory proliferation (Mcl-1$^{\Delta hep}$). The “classical” and widely used di-ethyl-nitrosamine (DEN) model was included, since it is generally considered to mimic toxin-induced cancerogenesis (7).

The aim of our study was to subtype HCC mouse models with different cancerogenesis backgrounds, to increase the translational value of rodent models. Based on comparative genomic hybridization (CGH) analysis, we propose a novel strategy to quantify the similarity of murine and human tumors. The starting criterion was the percentage of genomic overlap in the synteny analysis of CGH data of murine tumors compared to HCC patients of the TCGA database. Furthermore, we categorized histomorphological features and immunohistochemistry profiles to show different qualities and levels of overlap. Each set of murine tumors (DEN treatment, c-Myc induced, TAK1$^{LPC\text{-}KO}$ knock out, AlbLTαβ transgenic mice and Mcl-1$^{\Delta hep}$ knock out) was compared to three clinically defined subsets of human HCC (alcohol, chronic viral hepatitis, NASH/cryptogenic) and molecular subclasses G1-6, in order to

identify which rodent model recapitulates HCC carcinogenesis in specific etiologic backgrounds. Our approach might help future guidelines to stratify and compare preclinical mouse models – finally helping to increase the success rate in clinical trials.

Material and methods

Murine tissues

Formalin-fixed, paraffin-embedded (FFPE) mouse liver tissues retrieved from previous studies as listed in Table 1 were used (7, 10, 11, 16, 17). Original experiments with mice had been conducted in concordance with local guidelines (approval: “Tierversuchsgenehmigung vom Kantonalen Veterinäramt Zürich 63/2011”). Five mouse models were used: In the DEN models, tumors were chemically induced in wild type (C57BL6 strain) mice (7). The c-Myc model is a transgenic model targeting the c-Myc proto-oncogene (16). In the TAK1$^{LPC\text{-}KO}$ model, specific depletion of TAK1$^{LPC\text{-}KO}$ in liver parenchymal cells leads to deregulated TNF signaling as well as defective AMPK activation resulting in chronic mTORC1 activation (19). Liver cells undergo uncontrolled proliferation and necroptosis/apoptosis leading to early, accelerated liver cancer formation in mice (17, 20). The transgenic AlbLTαβ/tg+ referred to as AlbLTαβ model reflects inflammation-induced carcinogenesis with aberrant expression of the cytokine lymphotoxin (10). The Mcl-1$^{\Delta hep}$ model mimics chronic liver cell damage through liver-specific depletion of the anti-apoptotic protein myeloid cell leukemia 1 protein, which leads to continual hepatocyte apoptosis, increased cell turnover, compensatory proliferation and spontaneous tumor formation (8, 11).

Mutation analysis and comparative genomic hybridization

For mutation analysis and comparative genomic hybridization, CGH (n=75), DNA was extracted from FFPE tissues (Kit, GE-healthcare). PCR was performed with following the manufacturer's protocols (AmpliTaq Gold, Applied Biosystems), conducting 40 cycles (*TP53* exon 5-8, *CTNNB1*) or 35 cycles (*BRAF*, *HRAS*). Primer were used as previously described: *CTNNB1* exon 2 (21), *TP53* exon 5-8 (22), *HRAS* and *BRAF* (23). Annealing temperatures were 56°C (*TP53* exon 6 and 8, *BRAF*, *HRAS*) or 60°C (*TP53* exon 5 and 7). PCR amplification and sequencing of the mTERT core promoter fragment (24, 25) was performed on a subset of tumors (n=31 tumor samples) and 10 unaffected tissues. We used (-279 to +14 coverage) two primer pairs, forward1/2: TTA CTC CAA CAC ATC CAG CAA and CCT TCC GCT ACA ACG CTT; reverse 1/2: AAA GAT GAG GCT GGG AAC G and GAG CGC GGG TCA TTG TG at 58°C annealing temperature. Sequencing was performed using a commercial service (Microsynth Switzerland) with drop outs (1-10%) due to poor DNA quality. Mutation analysis was performed using Bioedit freeware, GRCm38/mm9 served as the reference genome. For CGH analysis, commercially available kits (Oligonucleotide Array-Based CGH for Genomic DNA Analysis, Agilent, Santa Clara, USA) were used (26), CGH results were matched with results from the TCGA cohort (TCGA-LIHC; http://cancergenome.nih.gov/. Synteny analysis of CGH data was performed according to the theory of eutherian chromosome evolution (27). Contingency tables were constructed with etiology-dependent HCC subsets such as alcohol-related, hepatitis B/C-induced or NASH-induced/cryptogenic HCC. Cryptogenic HCC were used for the analysis since these tumors are likely caused by burned out NASH even in the absence of cirrhosis (28-30). Fisher's exact test was used for statistical analysis, adjusted for multiple testing (Benjamini-Hochberg-correction). A significance level of 5% was set to detect significant correlations

between human and mouse chromosomal losses and gains controlling for the alpha error. The classification of hepatocellular carcinoma proposed by Boyault et al.(31) into the subgroups G1-G6 was applied to the Cancer Genome Atlas (TCGA) cohort. The dataset E-TABM-36 was retrieved from ArrayExpress (ebi.ac.uk/arrayexpress) and class labels were extracted from Fig. 1 of Boyault et al. An additional dataset, GSE62232, was retrieved from GEO (ncbi.nlm.nih.gov/geo), and class labels were kindly provided by the authors. A list of top overexpressed genes per subgroup was produced by comparing patients in each subgroup with patients in all other subgroups. These lists were then used to classify patients from the TCGA cohort into the 6 subgroups using the Nearest Template Prediction algorithm (32).

Morphology and immunohistochemistry

A systematic review of the documented murine models was performed (10, 11, 16, 17). For virtual microscopy, we digitalized images of murine liver lesions with available immunohistochemistry results (n=149) using a Nano Zoomer C9600 Virtual Slide Light microscope scanner by Hamamatsu using NDP, View Software, version 1.2.36.

Murine liver lesions were classified as tumors based on morphologic criteria reported by Thoolen et al. (9) and five markers of liver pathology (Fig. S1). Briefly, overgrowth compressing the normal tissue and/or distortion of the lobular architecture were considered as main criteria for malignant tumors in contrast to dysplastic nodules. Collagen IV loss or broadening of trabecular structures was regarded as neoplastic growth. Cytological features considered as indicators for malignancy were cell polymorphism, atypia, increased nucleus-cytoplasm ratio, inclusion bodies or basophilia. Sizes of cells and nuclei were measured using digitalized histological

pictures and dichotomized by the median. The tumor grading was based on a combination of nuclei sizes (<10µm=1, 10-15µm=2, 15-20µm=3), presence of nucleoli and cell-plasma ratio (decreased/normal). Proliferation in tumors was assessed as a 4-point scale (none, few, many, abundant).

Immunohistochemistry on mouse tissues (glutamine synthetase, A6, GP73, collagen IV, Ki-67) were performed as described (10, 17). For human liver tissues, stainings of glutamine synthetase, CK7 and CK19 were conducted and scored as reported (33). Positivity for a marker was defined as follows: A6 and CK7/19: >10% of tumor cells, glutamine synthetase: diffuse strong staining of >50% cells, GP73: weak or strong positivity. For statistical analysis of morphological features, immunohistochemistry and mutational profiles, SPSS software was used (IBM SPSS, Version 21).

Human tissues samples

Human liver tissues were retrieved from the archives and biobank of the Department of Pathology and Molecular Pathology, University Hospital Zurich. Tissue microarrays (TMA) with duplicates of a total of 61 HCC patients and 60 matched controls were used for immunohistochemical analysis as described (34). Follow-up data for all patients were available. The study was reviewed and approved by the Cantonal Ethics Committee of Zurich, Switzerland according to guidelines (KEK-ZH-Nr. 2013-0382).

Results

Tumor characteristics of different liver cancer mouse models

First, we aimed to perform a systematic histopathologic characterization comparing murine livers of all models (Table 2). Analysis of a total 49 mouse livers with an average of ~3 tumors per mouse (mean 3.04 1/- 0.81) revealed several differences among the five mouse models. Smaller, rather monomorphic tumors and numerous dysplastic lesions were found in the DEN-treated and TAK1^{LPC-KO} models, compared to larger, less abundant tumors in the c-Myc, the Mcl-1 $^{\Delta hep}$ and the AlbLTαβ models. In the Mcl-1$^{\Delta hep}$ model, subnodules were observed, which were reminiscent to those observable in human HCC (33). The size of cells and nuclei in individual tumors was higher in the TAK1^{LPC-KO} and AlbLTαβ models compared to others ($p < 0.01$). High grade tumors, defined by a combination of large nuclei, presence of nucleoli and an increased nuclear/cytoplasmatic ratio, were found in the TAK1^{LPC-KO} and the AlbLTαβ model (67% and 83% of tumors respectively). High proliferation was found in tumors of the Mcl-1$^{\Delta hep}$ model (21 tumors of total 38) and the c-Myc model (15 tumors of total 22).

Analysis of chromosomal gains and losses per mouse and tumor revealed patterns with predominant chromosomal gains (DEN, TAK1^{LPC-KO}) and patterns with predominant chromosomal losses (AlbLTαβ) (Figure 1A). In comparison to the unstratified TCGA reference HCC cohort, the percentage of combined aberrations (amplification and deletions) that overlapped between the murine tumors and human HCCs ranged from 56% in the TAK1^{LPC-KO} model to 71% (mean=61%) in the AlbLTαβ model (Table 2 and Figure 2).

Targeted mutational analysis of commonly affected genes (*TP53, HRAS, NRAS, CTNNB1, TERT*) yielded that murine liver tumors across all mouse models were *TP53* wild type (Figure 1B). 33% of analyzed DEN induced tumors showed *BRAF* mutations, lower than previously reported (35). *CTNNB1* were found in the c-Myc model (10%) and in four liver tumors (21%) of the same animal within the Mcl-1$^{\Delta hep}$ group. At low frequency (max. 11%), *HRAS* mutations (DEN, Mcl-1$^{\Delta hep}$ and c-Myc model) were detected. *TERT* promoter mutations of the transcription factor binding sites were not detected in a subset of murine tumor samples (n=31).

A subtype-specific approach based on CGH synteny analysis

By comparing CGH profiles of distinct HCC patient subsets from the TCGA database with profiles of each mouse model, the mean overlap further increased by maximally 14% (Figure 2A and B). Murine tumors of the DEN and c-Myc model shared genomic changes predominantly with alcohol induced HCCs (63-69%; $p<0.01$) and G5 molecular subclass. AlbLTαβ and TAK1$^{LPC\text{-}KO}$ resembled the closest NASH-HCC (57-67%, $p<0.01$) and G3 molecular subclass. Mcl-1$^{\Delta hep}$ showed highest overlap with viral hepatitis induced HCC (60%, $p<0.01$) and the G3 molecular subclass.

We next tested whether morphological findings support the CGH based classification of murine tumors (Figure 3A-C). In the DEN model, abundant cellular inclusions mimic Mallory-Denk bodies found in toxin-damaged liver cells. The presence of fatty change and clear cell cytology supports chronic nutritive-toxic liver cell damage. The c-Myc model was the second closest match for alcohol induced cancer, based on CGH analysis. Histopathological findings comprised clear cell features and pale

inclusion bodies in combination with lymphocyte infiltration and distorted lobular architecture (Figure 3B).

HCC of NASH/cryptogenic background matched closest with tumors from the TAK1^{LPC-KO} model and AlbLTαβ model (CGH analysis). Histopathology showed steatosis, massive lymphocyte infiltration and tumor necrosis in the AlbLTαβ model. NASH-typical morphological findings were less frequent in the TAK1^{LPC-KO} model, possibly due to the early onset of carcinogenesis in this model. In contrast, a frequent finding was the mixed-cell phenotype, consisting of side-by-side eosinophilic and basophilic cells typically found in rodents and indicative of liver damage.

Mcl-1$^{\Delta hep}$ tumors matched more closely to virus induced HCC than other etiologies based on CGH analysis (60%, $p<0.004$), and the greatest overlap was seen with patients with hepatitis B ($p<0.025$). Morphologically, tumors of the Mcl-1$^{\Delta hep}$ model showed apoptotic hepatocytes, highly proliferative tumors, tumor necrosis, steatosis and moderate lymphocyte infiltration. Of note, fibrosis was rare in non-tumorous liver tissue throughout all models.

***Inter*- and *intra*tumor heterogeneity**

Given that human HCC are mostly well-demarcated tumors with variable growth patterns and cytology, we next analyzed tumor growth including inter- and intratumor heterogeneity (32, 36). *Inter*tumor heterogeneity refers to the diversity of tumors within each model, and is defined by the number of histology pattern per mouse cohort. *Intra*tumor heterogeneity refers to the heterogeneity within each tumor, and is defined by histology patterns per individual tumor. As for the intertumor heterogeneity, we have analyzed it on morphology, immunohistochemistry and CGH

level. Two of the models (DEN and TAK1^{LPC-KO}) showed no tumor heterogeneity at all, whereas three models (Mcl-1$^{\Delta hep}$, c-Myc and AlbLTαβ) display tumor heterogeneity on CGH level and by histology. In detail, a single major growth pattern and maximum two cytological features were found in the DEN model and the TAK1^{LPC-KO} model. In contrast, two (c-Myc model) or more than three growth patterns (Mcl-1$^{\Delta hep}$ and AlbLTαβ model) in combination with cytological features were observed (*inter*tumor heterogeneity). *Intra*tumor heterogeneity (>2 different growth patterns and/or cytological features within the same tumor) was present in ~50% of Mcl-1$^{\Delta hep}$ and AlbLTαβ tumors. In three of the models (DEN, Mcl-1$^{\Delta hep}$, AlbLTαβ), tumors were clearly demarcated compared to a diffuse intrahepatic growth in the other two models i.e. c-Myc and TAK1^{LPC-KO} (Figure 3D).

Immunohistochemistry profiles

Next, we were wondering whether IHC profiles in murine liver tumors mimicked the profiles of human HCC. Homogeneous immunohistochemistry profiles were observed in the TAK1^{LPC-KO} model and the DEN-treated model. Tumors of the TAK1^{LPC-KO} model were nearly exclusively negative for A6 (biliary/progenitor phenotype) and glutamine synthetase indicating β-catenin activation (36). Tumors of the DEN-treated mice were A6 positive in 85%. Heterogeneous, more human-like profiles were present in the c-Myc and the Mcl-1$^{\Delta hep}$ model, including positivity for glutamine synthetase and/or A6. The closest resemblance of the HCC cohort immunohistochemistry profile was found in the AlbLTαβ model (Figure 4A and B).

In summary, murine tumors segregate into mainly biliary/progenitor-like phenotypes (DEN-treated, Mcl-1$^{\Delta hep}$), β-catenin-activated phenotype (c-Myc) and mixed

(AlbLTαβ). Table 3 shows a summary of IHC, genetic and morphological subtyping results.

Discussion

The challenge for future liver cancer models is to account for heterogeneity of disease, etiology-dependent pathogenesis and therapeutic targets. Our approach suggests that these aspects should be considered to improve the clinical relevance and translational value of preclinical cancer research models.

Taking advantage of comparative genomic hybridization (CGH), we were able to discriminate between preclinical models recapitulating alcohol induced, virus related and NASH-HCC as well as molecular subclasses G1-G6. By matching chromosomal aberrations of mouse and human tumors, it is possible to construct an algorithm to measure the concordance (p-value) of a model and a specific patient subgroup. As previously reported, synteny studies efficiently compare homologue mouse and human chromosomal aberrations (37). Sequencing of tumor suppressors and oncogenes might also be helpful to identify molecular markers, though mutational profiles of murine liver tumors largely differ from human HCC. For example, we found *BRAF* and *HRAS* mutations (rare in humans) as was reported in previous studies (23, 35). The absence of *TP53* mutations in murine tumors is in line with earlier findings (15) and stands in contrast to human HCC. *CTNNB1* mutations, found in 27% of human HCC regardless of their etiology (38) were only present in two models (c-Myc and Mcl-1$^{\Delta hep}$). Recently, a study with similar design as ours was performed by Dow et al. based on genomic and transcriptomic profiles in mouse vs. human tumor tissues (39). The authors claim that distinct mouse models reflect aspects of low grade human tumors, whereas e.g. DEN tumors carry a high mutational burden

similar to poorly differentiated tumors. Going beyond the molecular level, we have aimed to perform a comprehensive approach integrating morphological, immunohistochemistry and CGH analysis to assess human-mouse similarities.

The correlation of histopathological characteristics and CGH results we observed, supports the etiology oriented subtyping of HCC mouse models (33, 40, 41). A recent study of Calderaro et al. reported the relationship between heterogeneous histological subtypes and associated oncogenic pathways in HCC (42). As was demonstrated in our analysis, intracellular hyaline bodies are abundant in DEN-induced tumors that matched closest to alcohol induced HCC. The cellular inclusions are reminiscent of Mallory-Denk bodies, typical for human alcoholic steatohepatitis. The rounder hyaline bodies and irregular, keratin 8 containing Mallory bodies (43) coexisted in a study on 174 human HCC in 7.5% of cases (44). A crucial finding is also the presence of steatosis, indicative of metabolic deregulation (9) characteristic for NASH patients. NASH/cryptogenic HCC were best recapitulated by tumors of the AlbLTαβ and TAK1$^{LPC\text{-}KO}$ model. Particularly the AlbLTαβ model showed features diagnostic for NASH such as steatosis and inflammatory infiltration (45, 46) criteria for diagnosing NAFLD/NASH. Even though the model was originally developed to mimic human chronic viral hepatitis (10), the current analysis found more similarities with NASH-induced HCC. Fibrosis, an important feature of human chronic liver disease, was rare in murine tumors, as has been documented before (47).

It is one of the key observations of this study is that inter- and intratumor heterogeneity is present in varying degrees in HCC mouse models, which could be considered as an indicator of appropriateness murine models. While human HCC typically show inter-and intratumor heterogeneity (33), this feature is recapitulated only by particular liver cancer models (Mcl-1$^{\Delta hep}$, c-Myc and AlbLTαβ). Taking into

account inter- and intratumor heterogeneity in preclinical models, is crucial for many solid cancer models, especially for systemic treatment testings in advanced disease. Suitable preclinical animal models recapitulating diverse histopathology, immunohistochemistry profiles and associated oncogenic pathways of human HCC subtypes can be expected to better recapitulate treatment responsiveness.

A limitation of our study is that intratumor heterogeneity was analyzed only on the level of morphology and immunohistochemistry. In line with earlier findings, the phenotype-genotype correlations studies have shown that genetic heterogeneity frequently goes along with morphological and immune-phenotypic heterogeneity (33). Since we could not find morphological and/or immune-phenotypical intratumor heterogeneity except for nodule-in-nodule growth in one model (Mcl-1$^{\Delta hep}$), we did not follow up on microdissection of the lesions. Another limitation of our study regards imaging and treatment responses in preclinical models, that were performed in a study by Gross et al. (12) .This study compared the DEN model to the allograft model McA looking at tumor imaging in conjunction with histopathology, CGH and treatment response.

Regarding the recent interest in the immune microenviroment (48, 49) with focus on T-cells in NASH (37, 50), mainly the AlbLTαβ model seems to have potential for consecutive subtyping of lymphocytes and PD-L1 expression analysis. A response rate of 20% for PD-1 (anti-programmed cell death-1 antibody) monotherapy in phase I/II trials has been attributed to the refractory immune suppressive status in liver cancer patients (51), which needs further investigation.

In summary, contemporary preclinical models may be assigned to etiology-dependent patient groups and should account for inter-and intratumor heterogeneity.

This holds implications for the preclinical testing of targeted treatments and could improve patient management.

References

1. El-Serag HB, Kanwal F. Epidemiology of hepatocellular carcinoma in the United States: where are we? Where do we go? Hepatology. 2014;60:1767-75.
2. Torre LA, Bray F, Siegel RL, Ferlay J, Lortet-Tieulent J, Jemal A. Global cancer statistics, 2012. CA Cancer J Clin. 2015;65:87-108.
3. Mittal S, El-Serag HB. Epidemiology of hepatocellular carcinoma: consider the population. J Clin Gastroenterol. 2013;47 Suppl:S2-6.
4. Michelotti GA, Machado MV, Diehl AM. NAFLD, NASH and liver cancer. Nat Rev Gastroenterol Hepatol. 2013;10:656-65.
5. Ascha MS, Hanouneh IA, Lopez R, Tamimi TA, Feldstein AF, Zein NN. The incidence and risk factors of hepatocellular carcinoma in patients with nonalcoholic steatohepatitis. Hepatology. 2010;51:1972-8.
6. Gengenbacher N, Singhal M, Augustin HG. Preclinical mouse solid tumour models: status quo, challenges and perspectives. Nat Rev Cancer. 2017.
7. Maeda S, Kamata H, Luo JL, Leffert H, Karin M. IKKbeta couples hepatocyte death to cytokine-driven compensatory proliferation that promotes chemical hepatocarcinogenesis. Cell. 2005;121:977-90.
8. Vick B, Weber A, Urbanik T, Maass T, Teufel A, Krammer PH, et al. Knockout of myeloid cell leukemia-1 induces liver damage and increases apoptosis susceptibility of murine hepatocytes. Hepatology. 2009;49:627-36.
9. Thoolen B, Maronpot RR, Harada T, Nyska A, Rousseaux C, Nolte T, et al. Proliferative and nonproliferative lesions of the rat and mouse hepatobiliary system. Toxicol Pathol. 2010;38:5S-81S.

10. Haybaeck J, Zeller N, Wolf MJ, Weber A, Wagner U, Kurrer MO, et al. A lymphotoxin-driven pathway to hepatocellular carcinoma. Cancer Cell. 2009;16:295-308.
11. Weber A, Boger R, Vick B, Urbanik T, Haybaeck J, Zoller S, et al. Hepatocyte-specific deletion of the antiapoptotic protein myeloid cell leukemia-1 triggers proliferation and hepatocarcinogenesis in mice. Hepatology. 2010;51:1226-36.
12. Gross C, Steiger K, Sayyed S, Heid I, Feuchtinger A, Walch A, et al. Model Matters: Differences in Orthotopic Rat Hepatocellular Carcinoma Physiology Determine Therapy Response to Sorafenib. Clin Cancer Res. 2015;21:4440-50.
13. de La Coste A, Romagnolo B, Billuart P, Renard CA, Buendia MA, Soubrane O, et al. Somatic mutations of the beta-catenin gene are frequent in mouse and human hepatocellular carcinomas. Proc Natl Acad Sci U S A. 1998;95:8847-51.
14. Devereux TR, Anna CH, Foley JF, White CM, Sills RC, Barrett JC. Mutation of beta-catenin is an early event in chemically induced mouse hepatocellular carcinogenesis. Oncogene. 1999;18:4726-33.
15. Kress S, Konig J, Schweizer J, Lohrke H, Bauer-Hofmann R, Schwarz M. p53 mutations are absent from carcinogen-induced mouse liver tumors but occur in cell lines established from these tumors. Mol Carcinog. 1992;6:148-58.
16. Thorgeirsson SS, Santoni-Rugiu E. Transgenic mouse models in carcinogenesis: interaction of c-myc with transforming growth factor alpha and hepatocyte growth factor in hepatocarcinogenesis. Br J Clin Pharmacol. 1996;42:43-52.
17. Bettermann K, Vucur M, Haybaeck J, Koppe C, Janssen J, Heymann F, et al. TAK1 suppresses a NEMO-dependent but NF-kappaB-independent pathway to liver cancer. Cancer Cell. 2010;17:481-96.
18. Boege Y, Malehmir M, Healy ME, Bettermann K, Lorentzen A, Vucur M, et al. A Dual Role of Caspase-8 in Triggering and Sensing Proliferation-Associated DNA Damage, a Key Determinant of Liver Cancer Development. Cancer Cell. 2017;32:342-59 e10.
19. Inokuchi-Shimizu S, Park EJ, Roh YS, Yang L, Zhang B, Song J, et al. TAK1-mediated autophagy and fatty acid oxidation prevent hepatosteatosis and tumorigenesis. J Clin Invest. 2014;124:3566-78.
20. Vucur M, Reisinger F, Gautheron J, Janssen J, Roderburg C, Cardenas DV, et al. RIP3 inhibits inflammatory hepatocarcinogenesis but promotes cholestasis by controlling caspase-8- and JNK-dependent compensatory cell proliferation. Cell Rep. 2013;4:776-90.
21. Huang H, Ushijima T, Nagao M, Sugimura T, Ohgaki H. Beta-catenin mutations in liver tumors induced by 2-amino-3,4-dimethylimidazo[4,5-f]quinoline in CDF1 mice. Cancer Lett. 2003;198:29-35.

22. Calvert RJ, Tashiro Y, Buzard GS, Diwan BA, Weghorst CM. Lack of p53 point mutations in chemically induced mouse hepatoblastomas: an end-stage, highly malignant hepatocellular tumor. Cancer Lett. 1995;95:175-80.
23. Jaworski M, Buchmann A, Bauer P, Riess O, Schwarz M. B-raf and Ha-ras mutations in chemically induced mouse liver tumors. Oncogene. 2005;24:1290-5.
24. Greenberg RA, Allsopp RC, Chin L, Morin GB, DePinho RA. Expression of mouse telomerase reverse transcriptase during development, differentiation and proliferation. Oncogene. 1998;16:1723-30.
25. Pericuesta E, Ramirez MA, Villa-Diaz A, Relano-Gines A, Torres JM, Nieto M, et al. The proximal promoter region of mTert is sufficient to regulate telomerase activity in ES cells and transgenic animals. Reprod Biol Endocrinol. 2006;4:5.
26. Mu X, Espanol-Suner R, Mederacke I, Affo S, Manco R, Sempoux C, et al. Hepatocellular carcinoma originates from hepatocytes and not from the progenitor/biliary compartment. J Clin Invest. 2015;125:3891-903.
27. Wienberg J. The evolution of eutherian chromosomes. Curr Opin Genet Dev. 2004;14:657-66.
28. Caldwell SH, Oelsner DH, Iezzoni JC, Hespenheide EE, Battle EH, Driscoll CJ. Cryptogenic cirrhosis: clinical characterization and risk factors for underlying disease. Hepatology. 1999;29:664-9.
29. Ertle J, Dechene A, Sowa JP, Penndorf V, Herzer K, Kaiser G, et al. Non-alcoholic fatty liver disease progresses to hepatocellular carcinoma in the absence of apparent cirrhosis. Int J Cancer. 2011;128:2436-43.
30. Torres DM, Harrison SA. Nonalcoholic steatohepatitis and noncirrhotic hepatocellular carcinoma: fertile soil. Semin Liver Dis. 2012;32:30-8.
31. Boyault S, Rickman DS, de Reynies A, Balabaud C, Rebouissou S, Jeannot E, et al. Transcriptome classification of HCC is related to gene alterations and to new therapeutic targets. Hepatology. 2007;45:42-52.
32. Hoshida Y. Nearest template prediction: a single-sample-based flexible class prediction with confidence assessment. PLoS One. 2010;5:e15543.
33. Friemel J, Rechsteiner M, Frick L, Bohm F, Struckmann K, Egger M, et al. Intratumor heterogeneity in hepatocellular carcinoma. Clin Cancer Res. 2015;21:1951-61.
34. Malz M, Weber A, Singer S, Riehmer V, Bissinger M, Riener MO, et al. Overexpression of far upstream element binding proteins: a mechanism regulating proliferation and migration in liver cancer cells. Hepatology. 2009;50:1130-9.
35. He G, Dhar D, Nakagawa H, Font-Burgada J, Ogata H, Jiang Y, et al. Identification of liver cancer progenitors whose malignant progression depends on autocrine IL-6 signaling. Cell. 2013;155:384-96.

36. Hale G, Liu X, Hu J, Xu Z, Che L, Solomon D, et al. Correlation of exon 3 beta-catenin mutations with glutamine synthetase staining patterns in hepatocellular adenoma and hepatocellular carcinoma. Mod Pathol. 2016;29:1370-80.
37. Wolf MJ, Adili A, Piotrowitz K, Abdullah Z, Boege Y, Stemmer K, et al. Metabolic activation of intrahepatic CD8+ T cells and NKT cells causes nonalcoholic steatohepatitis and liver cancer via cross-talk with hepatocytes. Cancer Cell. 2014;26:549-64.
38. Cancer Genome Atlas Research Network. Electronic address wbe, Cancer Genome Atlas Research N. Comprehensive and Integrative Genomic Characterization of Hepatocellular Carcinoma. Cell. 2017;169:1327-41 e23.
39. Dow M, Pyke RM, Tsui BY, Alexandrov LB, Nakagawa H, Taniguchi K, et al. Integrative genomic analysis of mouse and human hepatocellular carcinoma. Proc Natl Acad Sci U S A. 2018;115:E9879-E88.
40. Friemel J, Rechsteiner M, Bawohl M, Frick L, Mullhaupt B, Lesurtel M, et al. Liver cancer with concomitant TP53 and CTNNB1 mutations: a case report. BMC Clin Pathol. 2016;16:7.
41. Zhai W, Lim TK, Zhang T, Phang ST, Tiang Z, Guan P, et al. The spatial organization of intra-tumour heterogeneity and evolutionary trajectories of metastases in hepatocellular carcinoma. Nat Commun. 2017;8:4565.
42. Calderaro J, Couchy G, Imbeaud S, Amaddeo G, Letouze E, Blanc JF, et al. Histological subtypes of hepatocellular carcinoma are related to gene mutations and molecular tumour classification. J Hepatol. 2017;67:727-38.
43. Mahajan V, Klingstedt T, Simon R, Nilsson KP, Thueringer A, Kashofer K, et al. Cross beta-sheet conformation of keratin 8 is a specific feature of Mallory-Denk bodies compared with other hepatocyte inclusions. Gastroenterology. 2011;141:1080-90 e1-7.
44. Denk H, Stumptner C, Fuchsbichler A, Muller T, Farr G, Muller W, et al. Are the Mallory bodies and intracellular hyaline bodies in neoplastic and non-neoplastic hepatocytes related? J Pathol. 2006;208:653-61.
45. Brunt EM, Kleiner DE, Wilson LA, Belt P, Neuschwander-Tetri BA, Network NCR. Nonalcoholic fatty liver disease (NAFLD) activity score and the histopathologic diagnosis in NAFLD: distinct clinicopathologic meanings. Hepatology. 2011;53:810-20.
46. Caldwell SH, Lee VD, Kleiner DE, Al-Osaimi AM, Argo CK, Northup PG, et al. NASH and cryptogenic cirrhosis: a histological analysis. Ann Hepatol. 2009;8:346-52.
47. Reiberger T, Chen Y, Ramjiawan RR, Hato T, Fan C, Samuel R, et al. An orthotopic mouse model of hepatocellular carcinoma with underlying liver cirrhosis. Nat Protoc. 2015;10:1264-74.
48. Heikenwalder M, Pikarsky E. Learning the Roles of the Hepatic Adaptive Immune System in Hepatocellular Carcinoma-Nature's Guide for Successful Cancer Immunotherapy. Semin Liver Dis. 2017;37:210-8.

49. Pikarsky E, Heikenwalder M. Focal and Local: Ectopic Lymphoid Structures and Aggregates of Myeloid and Other Immune Cells in Liver. Gastroenterology. 2016;151:780-3.
50. Shalapour S, Lin XJ, Bastian IN, Brain J, Burt AD, Aksenov AA, et al. Inflammation-induced IgA+ cells dismantle anti-liver cancer immunity. Nature. 2017;551:340-5.
51. Nishida N, Kudo M. Immune checkpoint blockade for the treatment of human hepatocellular carcinoma. Hepatol Res. 2018.

Figure 1 Genomic landscapes of murine liver tumors assessed by comparative genomic hybridization (CGH) and targeted sequencing (A) Unsupervised clustering of genomic aberrations of single mouse tumor samples. Left column declares type of mouse model with malignant liver tumor on C57Bl/6 background (DEN; DEN induced, Myc; c-Myc, TAK; TAK1^{LPC-KO}, LT; AlbLTαβ and MCL; Mcl-1$^{\Delta hep}$). Color display shows chromosomal gains and losses per tumor (RED: losses, BLUE: gains). Each line represents one samples (i.e. one mouse). Samples are clustered by genetic similarities. (B) Sequencing results of targeted sequencing for most common gene altered in human HCC. Each square represents a sample (i.e. one murine tumor), squares are summarized by model including 1-3 control samples (wild type). Black squares indicate mutations, crossed out grey squares indicate that sample could not be sequenced due to quality reasons.

Figure 2 Etiology-dependent subtype approach of matching murine and human liver tumors based on CGH (A) Circular plots of synteny analysis comparing chromosomal aberrations of murine (M1-19) and human (H1-22) liver tumors. Inner circle (red) shows losses, outer circle (blue) shows gains. The closest match for the etiology dependent patient subset (bottom line) and each mouse model is represented by the combined matches of gains and losses.(B) Combined matches (gains and losses) of each model compared to the TCGA HCC cohort (LIHC, http://cancergenome.nih.gov/): etiology oriented patient subsets (green, upper heat map) as well as molecular subclasses (Boyault et al. 2007) G1-

G6 (red, lower heat map). Colors indicate concordance as follows: light green/red (<50%), green/red (>50%) and dark green/red (>60% or >70%). “All etiologies” comprises matching of genomic changes accounting for the unstratified TCGA set of human HCC. Numbers increase with specificity of genomic aberrations.

Figure 3 Growth patterns, cytological features and immune infiltration of murine liver tumors. (A) Histological patterns ranging in murine tumors (TAK1^{LPC-KO} and DEN, c-Myc, AlbLTαβ and Mcl-1$^{\Delta hep}$), involving solid growth, clear cell cytology and fatty change. Scale bars (overview) indicate 1mm (overviews) and 50µm (30x magnification). (B) Summarized features of tumor architecture, growth patterns and cytological features of murine liver tumors and (C) surrounding liver tissue. Heatmap indicates a semiquantitative analysis of respective histological features in number of murine tumors (faint red: not present-up to dark red: feature present in all/almost all tumors). (D) Schematic illustration of tumor heterogeneity and tumor borders in different murine models

Figure 4 Immunohistochemistry profiles of human versus murine liver tumors (A) Immunohistochemistry profiles of n=61 HCC patients depicted by stacked bar plots. Profiles were assessed by duplicate tissue microarray spots for glutamine synthetase (GS-indicating β-catenin activation) and CK7/CK19 stainings indicating stem-like phenotypes. ***-/-*** was used if none of the two marker was positive. Numbers declare percentages of tumors showing positivity for respective marker. Pictures show representative stainings of three HCCs: HCC1 CK7+ and GS-, associated to alcohol abuse. HCC2 represents GS+ and CK7- group, associated to hepatitis C. HCC3 represents the double negative group, the patient had none of the known risk factors (cryptogen). Scale bar indicates 50 µm in 30x magnification. (B) Immunohistochemistry profiles illustrated

by stacked bar plots of murine liver lesions classified as “tumors”, grouped by model. A6 is considered to correspond to CK7 in humans. GS: glutamine synthetase. Neg A6/GS was used if none of the two marker was positive. Numbers declare percentages of tumors showing positivity for the respective marker. Subnodules, i.e. tumor regions with different immunophenotypes within larger lesions were included in the analysis.

Table 1 Genetic background and phenotypic presentation of mouse models

Model	Genetic background	Mode	Phenotype of tumors as originally documented	Phenotype of surrounding liver tissue as originally documented	Average age at tumor development	Reference
DEN wt	C57BL/6/129	Chemically induced DNA (di-ethylnitrosamine)	Incidence lower in female animals and younger animals, typical liver histology	Liver injury and cell death, proliferative response	8-10 months	Maeda et al. 2005
c-Myc	C57BL/6J-CBA/J	Transgenic model with oncogene overexpression leading to genomic instability	Solid or trabecular histological type, atypia, polymorphism, hemorraghic necrosis	Transition of mild to severe dysplasia in hepatocytes, benign lesion ("Adenoma")	12-15 months	Thorgeirsson et al. 1996
$TAK1^{LPC\text{-}KO}$	C57BL6-SV129Ola	Knockout model with TAK1 deficiency, enhanced liver cell proliferation	Ductopenia, fibrosis, liver cell apoptosis, necrosis, hyperproliferation	Expansive growth, high cellularity, anisokaryosis of hepatocytes	4 months	Bettermann et al. 2010 Vucur et al. 2013
AlbLTαβ	CL57BL/6	Transgenic model with overexpression of cytokines, indirectly leading to cell damage	Multicentric nodules in tg 1223 mice, high proliferation, loss of Collagen IV network	Infiltration of lymphocytes and macrophages, increased proliferation (A6 cells)	12 months	Haybaeck et al. 2009
$Mcl\text{-}1^{\Delta hep}$	C57BL/6	Deficieny of antiapoptotic Mcl-1 with enhanced liver cell apoptosis, hyperproliferation	Altered liver architecture, cellular atypia, loss of Collagen IV, immunoreactivity for Glutamine synthethase	Apoptosis, pericellular fibrosis, enhanced proliferation	12 months	Vick et al 2009, Weber et al. 2010 Boege et al. 2017

Table 2 Histomorphology and genetic characterization of murine liver tumors

Model	No. of tumors (n=149)	No. of dysplastic lesions	Mean tumor size (mm)	Mutations[a] n=73	CGH based similarity to human HCC[b]	P-value CGH matches	Mean cell size (µm)	Mean size of nuclei (µm)	Proliferating tumors
DEN	19	146	3 +/-1.4	*BRAF* 3/9	60.8 (losses)	< 0.0001	25 +/- 5	10 +/- 1.4	44%
				HRAS 1/9	65.8 (gains)	0.636			
c-Myc	22	10	6.9 +/-3.8	*CTNNB1* 2/19	54.1 (losses)	< 0.0001	30 +/-7.5	10 +/-2.2	68%
				HRAS 1/19	57.5 (gains)	< 0.0001			
TAK1^{LPC-KO}	37	118	2.9 +/-1.7	None (wt 0/15)	47 (losses)	< 0.0001	40 +/- 10	14 +/- 4.6	9%
					61.8 (gains)	< 0.0001			
AlbLTαβ	33	2	6.6 +/-3.3	None (wt 0/11)	53.3 (losses)	0.1279	39 +/- 11	14 +/- 3.92	46%
					72.3 (gains)	< 0.0001			
Mcl-1$^{\Delta hep}$	38	79	5.6 +/-4.96	*BRAF* 4/19	62.8 (losses)	< 0.0001	32 +/-7	10 +/- 1.9	55%
				CTNNB1 4/19	63.7 (gains)	0.113			

[a] mutations tested in subset, genes: *BRAF, HRAS, CTNNB1, TP53 (Exon 5-8), TERT*

[b] percentages given by synteny analysis of murine tumors (n=75) and unstratified human HCC cohort (TCGA)

Table 3 Summary of mouse model subtyping results in comparison with respective HCC patient subsets (TCGA)

Model	Etiology based CGH/Synteny	G1-G6 groups CGH/synteny	Histologic features	Immunohistochemistry profiles	Immune infiltration	Inter-/intratumor heterogeneity
DEN	Alcohol-induced	G3/G5	Inclusion bodies, fibrosis (in tumors), steatosis	Only Stem/biliary-like phenotypes	Scarce	No/No
c-Myc	Alcohol-induced	G5	Pleomorphism, clear cell foci	WNT activation	Moderate	Yes/No
AlbLTαβ	NASH-associated	G3	Fatty change, steatosis, massive lymphocyte infiltration	Stem/biliary-like **>**WNT activation	Severe	Yes/Yes
$TAK1^{LPC\text{-}KO}$	NASH-associated	G3/G5	Signs of liver injury (eosinophilic change)	**No** WNT activation **No** Stem/biliary-like	Scarce	No/No
$Mcl\text{-}1^{\Delta hep}$	Viral hepatitis	G3	Highly proliferative, steatosis, fatty change, lymphocyte infiltration	Stem/biliary-like**>>**WNT activation	Moderate	Yes/Yes

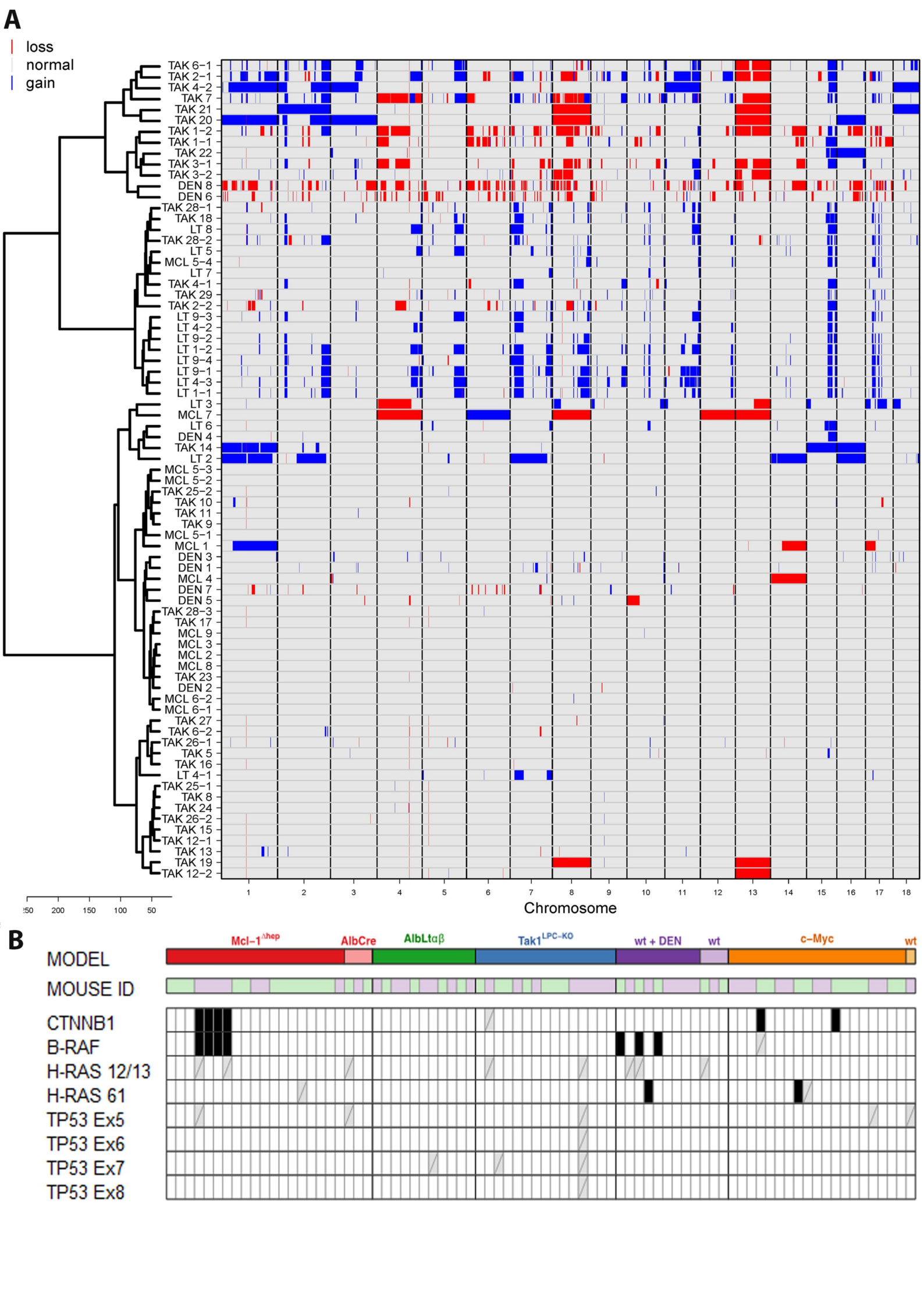
A
loss
normal
gain
TAK 6−1
TAK 2−1
TAK 4−2
TAK 7
TAK 21
TAK 20
TAK 1−2
TAK 1−1
TAK 22
TAK 3−1
TAK 3−2
DEN 8
DEN 6
TAK 28−1
TAK 18
LT 8
TAK 28−2
LT 5
MCL 5−4
LT 7
TAK 4−1
TAK 29
TAK 2−2
LT 9−3
LT 4−2
LT 9−2
LT 1−2
LT 9−4
LT 9−1
LT 4−3
LT 1−1
LT 3
MCL 7
LT 6
DEN 4
TAK 14
LT 2
MCL 5−3
MCL 5−2
TAK 25−2
TAK 10
TAK 11
TAK 9
MCL 5−1
MCL 1
DEN 3
DEN 1
MCL 4
DEN 7
DEN 5
TAK 28−3
TAK 17
MCL 9
MCL 3
MCL 2
MCL 8
TAK 23
DEN 2
MCL 6−2
MCL 6−1
TAK 27
TAK 6−2
TAK 26−1
TAK 5
TAK 16
LT 4−1
TAK 25−1
TAK 8
TAK 24
TAK 26−2
TAK 15
TAK 12−1
TAK 13
TAK 19
TAK 12−2
1
2
3
4
5
6
7
8
9
10
11
12
13
14
15
16
17
18
Chromosome
250
200
150
100
50
B
MODEL
MOUSE ID
Mcl−1Δhep
AlbCre
AlbLtαβ
Tak1LPC−KO
wt + DEN
wt
c−Myc
wt
CTNNB1
B-RAF
H-RAS 12/13
H-RAS 61
TP53 Ex5
TP53 Ex6
TP53 Ex7
TP53 Ex8

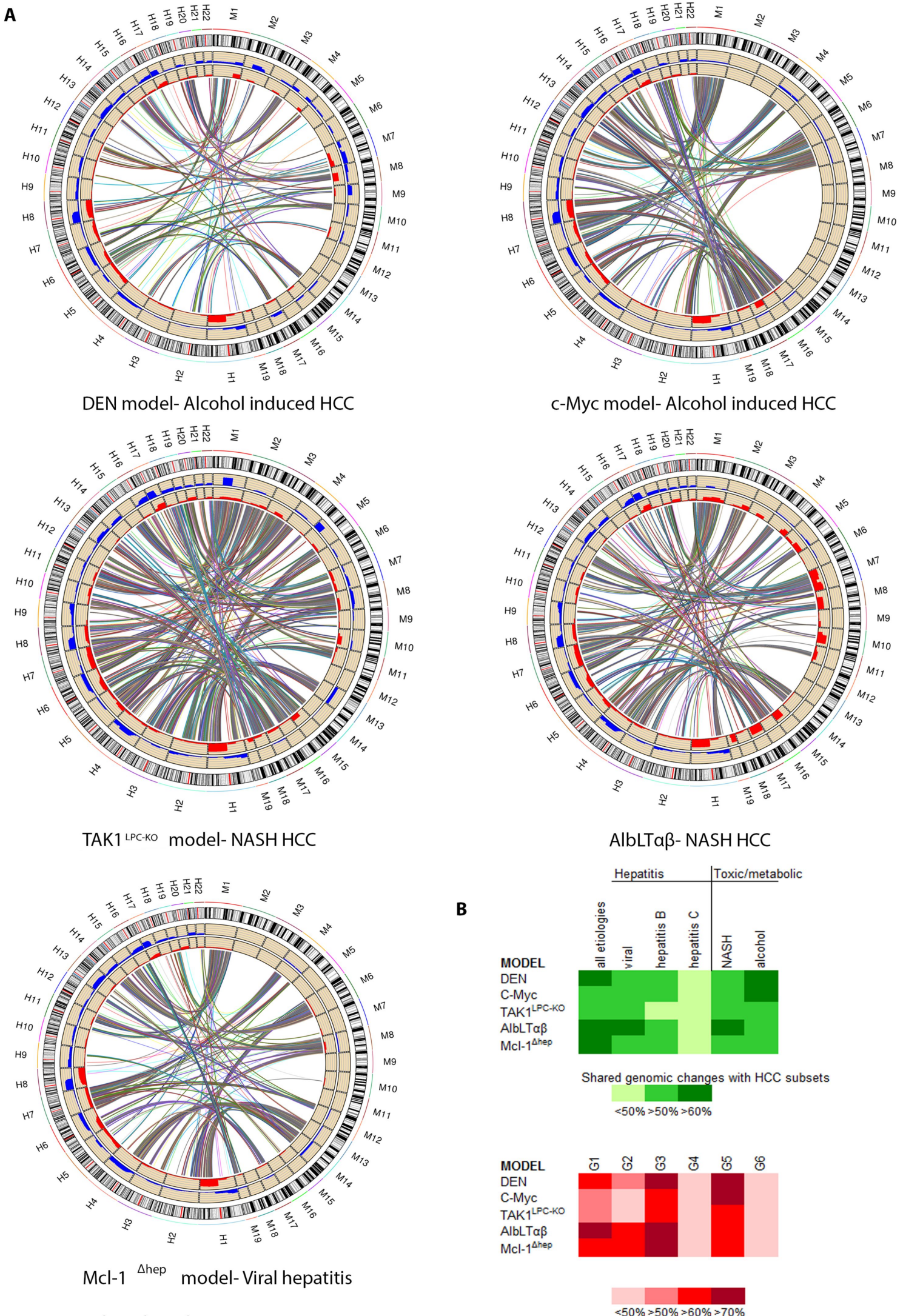

Figure 2 Friemel, Frick et al.

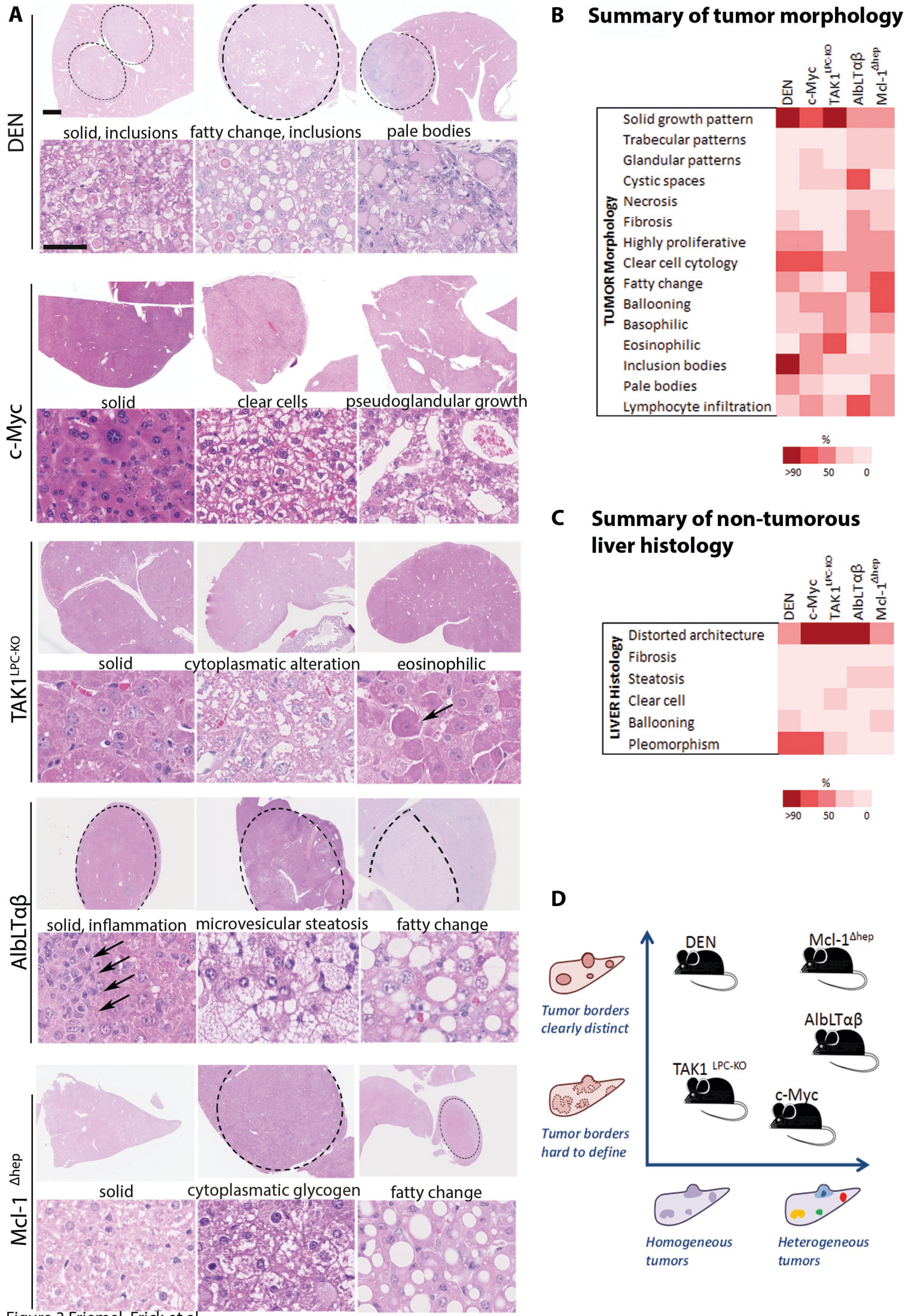

Figure 3 Friemel, Frick et al.

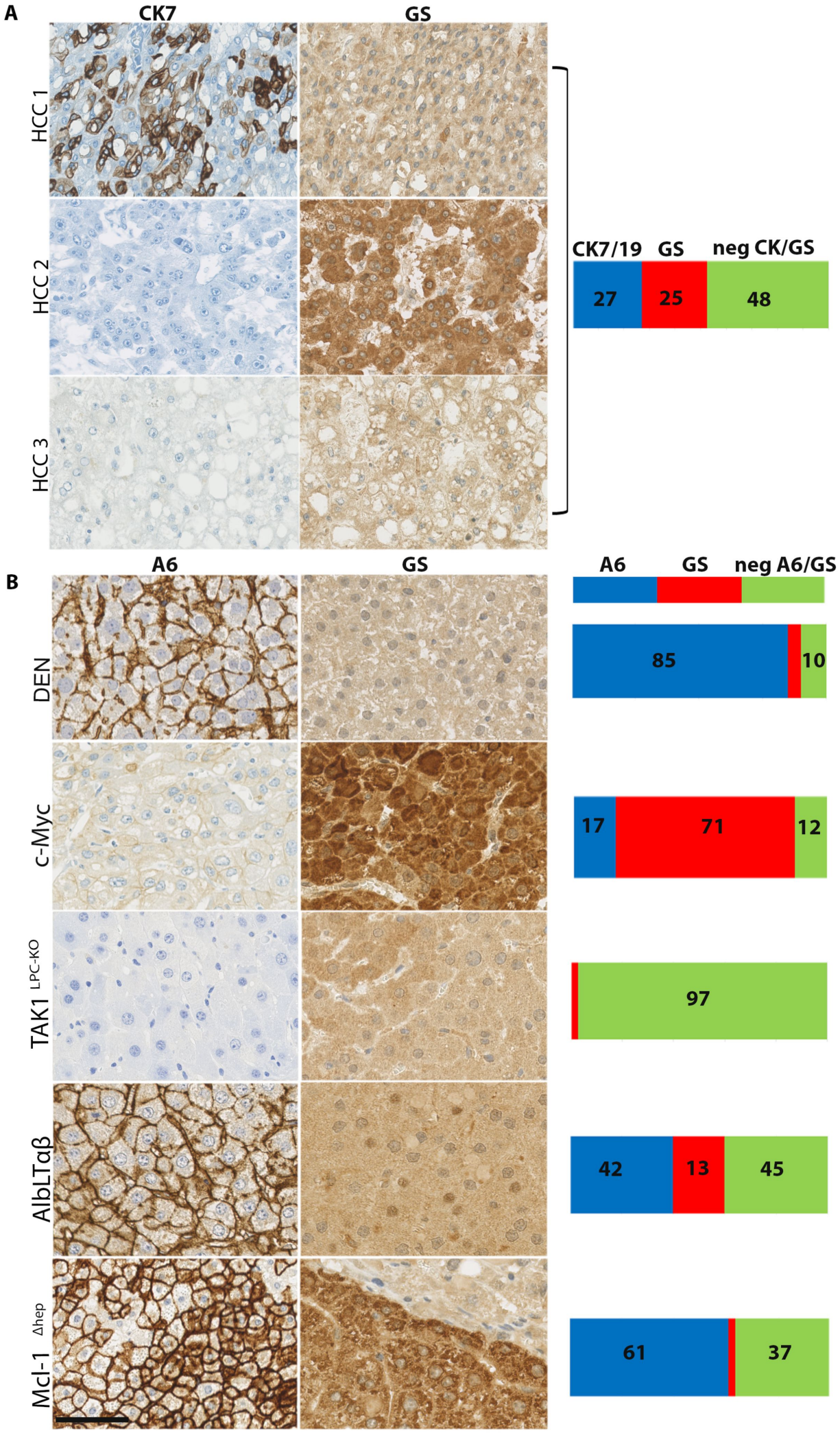

Figure 4 Friemel,Frick et al.